Shallow landslide susceptibility assessment in a data-poor region of Guatemala (Comitancillo municipality)

Federico Preti,[1] Tommaso Letterio[2]

[1]Engineering for Agro-Forestry and Biosystems Division, Department of Agricultural, Food Production and Forest Management, University of Florence; [2]Land reclamation consortium for Emilia-Romagna water channel, Bologna, Italy

Abstract

Although landslides are frequent natural phenomena in mountainous regions, the lack of data in emerging countries is a significant issue in the assessment of shallow landslide susceptibility. A key factor in risk-mitigation strategies is the evaluation of deterministic physical models for hazard assessment in these data-poor regions. Given the lack of physical information, input parameters to these data-intensive deterministic models have to be estimated, which has a negative impact on the reliability of the assessment. To address this problem, we examined shallow landslide hazard in Comitancillo municipality, Guatemala. Shallow landslides are here defined as small (less than two or three metre-deep) rotational or translational slides or earth flows. We based our hazard simulation on the stability index mapping model. The model's input parameters were estimated from a statistical analysis of factors affecting landslides in the municipality obtained from a geodatabase. The outputs from the model were analysed and compared to an inventory of small-scale landslides. The results of the comparison show the effectiveness of the method developed to estimate input parameters for a deterministic model, in regions where physical data related to the assessment of shallow landslide susceptibility is lacking.

Correspondence: Federico Preti, Engineering for Agro-Forestry and Biosystems Division, Department of Agricultural, Food Production and Forest Management (GESAAF), University of Florence, via San Bonaventura 13, 50145 Florence, Italy.
E-mail: federico.preti@unifi.it

Key words: Shallow landslides; Guatemala.

Acknowledgements: the authors would like to thank Dr. Francesco Anichini for his support during field monitoring activities and the *Italian Research Project of Relevant Interest (PRIN2010-2011), prot. 20104ALME4, National network for monitoring, modeling, and sustainable management of erosion processes in agricultural land and hilly-mountainous area.*

Received for publication: 23 January 2015.
Accepted for publication: 30 May 2015.

Journal of Agricultural Engineering 2015; XLVI:450
doi:10.4081/jae.2015.450

Introduction

Various natural disasters in recent centuries in Central America have been caused by landslides and debris flows (Zaitchik and van Es, 2003; Petley *et al*., 2005; Devoli *et al*., 2007a, 2007b; Medina, 2007; Miner and Villagran de Leon, 2008; Devoli *et al*., 2009). For example, in early October 2005 at the end of the rainy season, a storm system led to heavy rainfall in Guatemala (UNEP, 2005) and resulted in several landslides that had a severe impact on communities. More than 1800 people died (Cepeda *et al*., 2010) and the landslides that hit the Sololà and San Marcos Departments wrecked entire villages (Medina, 2007). However, the municipality of Comitancillo (San Marcos Department) escaped the disaster. There were no large-scale land movements (MAGA, 2001), although several shallow landslides and/or earthflows were observed. Nevertheless, landslides are the most significant cause of denudation in watersheds with steep slopes (Wentworth, 1943; Scott and Street, 1976; Li, 1988; Terlien, 1997; Lan *et al*., 2004).

Most landslides in Central and South America occur (or have the potential to occur) in mountainous regions of the Andes and steep slopes in volcanic regions. In rural zones of Guatemala, forested land has been degraded (Medina, 2007) or partially converted to subsistence agriculture (Bresci *et al*., 2013). Such changes in land use and land cover affect soil cohesion and critical pore water pressure, causing loss of root reinforcement and reduction of the canopy effect on interception and evapotranspiration (Kuriakose *et al*., 2009).

In the municipality the factors affecting landslides have never been identified or analysed; they include lithology, soil texture, slope angle, elevation (Lan *et al*., 2004; Ghosh *et al*., 2012; Jaiswal and van Westen, 2013; Pellicani *et al*., 2013) and vegetation (Glade, 2003). This is despite the fact that large-scale land movements pose a serious threat to life, property and infrastructure, and constrain the development of rural areas (Cepeda *et al*., 2010).

Several models have been proposed for assessing shallow landslide hazards at regional scale. Most all of these models couples a terrain-based distributed hydrological model for assessing the spatial distribution of soil moisture with an infinite-slope stability model for assessing the local stability factor. The spatial distribution of soil wetness conditions is generally predicted under the assumption that subsurface flow is driven by terrain gradients under steady state conditions. Under this assumption the local wetness conditions are univocally defined by means of terrain attributes, such as the upslope contributing area and the terrain slope.

The distributed model is generally structured on a network of elements defined by digital terrain analysis, either contour or grid-based (*e.g*., Chirico *et al*., 2003; Santacana *et al*., 2003). The elements are characterised by specific attributes structured in a digital terrain model. The connectivity among the elements is defined by one-dimensional flowpath patterns. Montgomery and Dietrich (1994), in their SHALSTAB model (Dietrich *et al*., 1992, 1993, 1995, 2001; Dietrich and

Montgomery, 1998), calculated the wetness patterns with a steady-state wetness index computed with a single-flow direction algorithm. Borga *et al*. (1998) extended this approach to grids with a multiple-flow-direction algorithm. Pack *et al*. (1998) included a parameter uncertainty analysis based on uniform probability distributions in order to assess the stability classes. Other models have been designed to relax the steady-state assumption, by implementing fully distributed hydrological dynamic models. Wu and Sidle (1995) applied a contour-based distributed event model. Borga *et al*. (2002) first suggested applying the quasi-dynamic wetness index (Barling *et al*., 1994) to overcome the limitations of the steady-state approach. Other examples of fully dynamic models are TRIGRS (Baum *et al*., 2002, 2008, 2010), SHETRAN (Bathurst *et al*., 2007) and STARWARS/PROBSTAB (van Beek and van Asch, 2004). The distributed fully dynamic models, although being able to account for realistic rainfall patterns, are computationally complex, require a large number of input data and parameters and do not have the practical advantages of an index-based approach. The largest source of uncertainty in these models is the estimation of the soil hydraulic properties affecting the celerity of the subsurface flow response, even at small hillslope scale (*e.g*., Chirico *et al*., 2010). Moreover, steady state approaches, can be easily implemented within GIS environments (Iverson, 2003). Another advantage of steady state model is the fact that they can easily incorporate the role of vegetation on slope stability (Preti and Giadrossich, 2009; Schwarz *et al*., 2009; Preti *et al*., 2010; Preti, 2013). Given the lack of available data as input to this data-intensive model, input parameters had to be estimated, we selected the SINMAP model in order to carry out a shallow landslide hazard assessment. The SINMAP model has been tested under different geological and hydrological conditions by several authors, and has proved to be highly reliable in predicting slope instabilities (Morrissey *et al*., 2001; Zaitchik and van Es, 2003; Calcaterra *et al*., 2004; Lan *et al*., 2004; Meisina and Scarabelli, 2007; Andriola *et al*., 2009). Model parameters have been derived from data published in common geodatabase for the area. A preliminary statistical analysis of factors affecting landslides was performed. The model was validated using an inventory of 24 landslide events.

This paper is organised as follows: the next section describes the characteristics of the case study, by focusing on the factors that affect landslides and describing the landslide inventory. Main features of the model are described and, specifically, an analysis of the triggering factors as input the model is provided. In section three, we evaluate the results of the landslide inventory analysis and discuss our findings.

Materials and methods

Study area

The study area is the Comitancillo municipality in the San Marcos Department of Guatemala. The total surface area is 139 km^2 and there are three watersheds. Seventy per cent of the bedrock is composed of volcanic rock; in particular, there are levels of ash, lava and lapillus.

According to Simmons *et al*. (1959), the soils in Comitancillo municipality belong mainly to the Andisol order of soil taxonomy with good/excessive drainage and a high risk of erosion. Soils developed on volcanic rock have a depth of 0.5-1.5 m and have a clay loam, loam and sandy loam texture. With respect to land use, 48% of the land is used for crop production, while 46% is covered by forest and shrub. According to the Köppen-Geiger classification, the climate in the San Marco Department is the subtropical highland variety (Cwb); it is humid, with cool, dry winters and mild summers.

Landslide-affecting factors

The first step in a landslide susceptibility analysis is data collection and evaluation. The geodatabase that formed the basis for our study contains data related to the variables that affect the risk of landslide (Lan *et al*., 2004). In order to estimate the input parameters for the SINMAP model we carried out a statistical analysis of the landslide-affecting factors contained in the database. Specifically, we selected and defined three categories of factors: slope angle, soil texture and soil cover. The 20-metre digital elevation model (DEM) (MAGA, 2001) was used to create the slope map. Slope angles were divided into four classes: 0°-10°, 10°-20°, 20°-30°, >30°. This classification was based on the results of Coe *et al*. (2004), who found that landslides tended to occur in areas with a slope angle of 20°-30°, while areas with a slope angle of 0-10° were less affected.

Soil texture was classified into clay loam, loam and sandy loam based on soil data. A land use map was used to evaluate areas covered by vegetation, as root-induced cohesion has been identified as the most important beneficial mechanical factor in shear strength (Greenway, 1987; Montgomery *et al*., 2000; Kuriakose *et al*., 2009; Preti and Giadrossich, 2009; Schwarz *et al*., 2009; Preti *et al*., 2010; Preti, 2013).

Landslide inventory

In Guatemala as a whole, 553 landslides were recorded in the period 1881-1981 (INSIVUMEH, 1991). However, in politically unstable years (such as during military coups) this number seems to be underestimated (Cepeda *et al*., 2010). There was an increase in the incidence of landslides in 1935 due to the expansion of the road network. No landslides have been mapped in the Comitancillo municipality. The scientific literature does not suggest that in the recent past, landslides in Guatemala have become any more frequent.

A 2009 survey determined the location of 25 shallow landslides using a global positioning system device (Figure 1). This two-month project focused on socio-economic features related to the large-scale movement of land and led to the creation of a landslide inventory. Landslides were classified as shallow rotational or translational, covering a surface area of 50-150 m^2.

The stability index mapping model

The stability index mapping (SINMAP) model, developed by Pack *et al*. (1998), integrates an infinite slope stability model and a steady-state hydrologic model, based on TOPMODEL (Beven and Kirkby, 1979; Connell *et al*., 2001). A detailed discussion of the SINMAP model is presented in Pack *et al*. (1998). Here we focus on a few key aspects of the model. In the absence of actual data, the set of variables and parameters of the infinite slope stability model is aggregated and become calibration input (Pack *et al*., 1998; Deb and El-Kadi, 2009; Kuriakose *et al*., 2009). The formulation of the stability equation for each DEM grid cell in the SINMAP model is:

$$FS = \frac{C + \cos\theta \cdot \left[1 - \min\left(\frac{R}{T} \cdot \frac{a}{\sin\theta}, 1\right) r\right] \cdot \tan\phi}{\sin\theta} \quad (1)$$

where: *FS* represents the safety factor; *C* [-] groups cohesion factors; ϕ is the angle of internal friction [°]; θ is the slope angle [°]; *R* and *T* are, respectively, water recharge [m/d] and transmissivity [m^2/d]; *r* is a constant; and *a* is the contributing area per unit contour length according to TOPMODEL (Beven and Kirkby, 1979). The cohesion index C (Pack *et al*., 1998) is expressed by the relation:

$$C = \frac{c_s + c_r}{h\gamma_s} \quad (2)$$

where: c_s [Pa] represents soil cohesion; c_r [Pa] is root cohesion; γ_s (N/m^3) is soil-specific weight; and h [m] is soil thickness.

Topographic variables (a and θ) are derived from the DEM, while the values of r, C, tan ϕ and R/T ([m/d]/[m^2/d]), are assigned by users. Uncertainty in the three variables C, tan ϕ, and R/T is modelled by the specification of upper and lower bounds (Deb and El-Kadi, 2009). The definition of input parameters makes it possible to classify the study area into various slope-stability classes. The SINMAP stability index (SI) is derived from the safety factor (FS) and is defined as the probability that a location is stable, assuming a uniform distribution of uncertain or variable parameters over a specified range. The SINMAP model defines the following zones: i) Class 1: a *stable slope* (SI>1.5); ii) Class 2: a *moderately stable slope* (1.5>SI>1.25); iii) Class 3: a *quasi-stable slope* (1.25>SI>1.0); iv) Class 4: a *lower threshold slope* (1.0>SI>0.5); v) Class 5: an *upper threshold slope* (0.5>SI>0.0); and vi) Class 6: a *defended slope* (0.0>SI). For more details see Pack *et al.* (1998). Consequently, when FS_{min}>1 the area can be classified as either *stable*, *moderately stable* or *quasi-stable*, while in the case of FS_{max}<1 the area is classified as unstable (*defended*).

Landslide-affecting factor analysis and model input

A preliminary analysis of the factors affecting the risk of landslide in the Equation 2.1 was carried out at the level of the municipality in order to evaluate the main slope processes. The SINMAP assessment is based on a statistical analysis of the factors affecting the risk of landslide. Three calibration regions, each covering 40 km^2 were identified, according to soil class distribution (Figure 2).

Figure 1. Map of soil angle classes and location of landslide inventory (red points) in Comitancillo municipality (Guatemala).

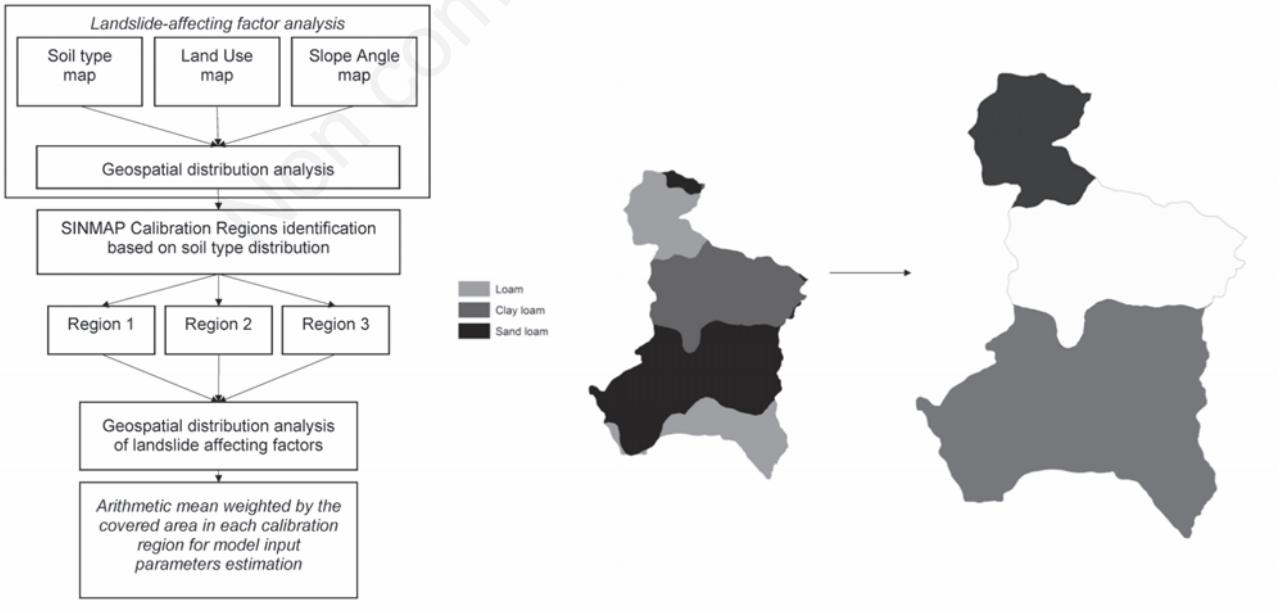

Figure 2. The process for model input estimation and evaluation according to land use, soil type and slope angle. In the first stage, a geostatistical analysis of factors affecting landslides was carried out. Three calibration regions were selected according to soil type distribution, and for each calibration region a geostatistical analysis was carried out. The model input parameters were calculated as the weighted arithmetic average of factors affecting landslides in the covered areas (Comitancillo, Guatemala; Lat: 15.09164, Long: –91.749444).

The calculated distribution of slope angle classes was used in the analysis of the frequency distribution of soil classes and land use (Figure 3). Table 1 shows the results of these calculations. Slopes with an angle less than 10°, 10°-20° and 20°-30° cover, respectively, around 15%, 32% and 34% of the total area (Figure 3).

Specific statistical analyses were carried out in each calibration region (CR) to verify the homogeneity of the area and to evaluate its landslide-affecting factors (Figure 3). For example, in CR3, areas with a slope angle greater than 20° cover only 14.8% of the total area, while in CR1 and CR2 they cover 53.8% and 71.3%, respectively. In CR2 shrub cover dominates, occupying 69.1% of the area (Table 2). In the right part of Figure 3 the distribution of landslide-affecting factors for the three calibration regions expressed as a percentage is shown,

Maximum daily rainfall was calculated from rainfall data provided by the meteorological gauge station in San Marcos city (daily rainfall records covering a period of 39 years). This was used to evaluate the input parameter *R* for each CR (Deb and El-Kadi, 2009).

The soil texture in each CR was assessed using the soil map and was used to calculate low-threshold hydraulic conductivity (Ks_{min}) using Cosby's pedotransfer function (Cosby *et al*., 1984). The values of Ks_{max} were estimated by application of the Philip formula (Philip, 1957) for the calculation of infiltration rate as a function of time (starting at 0.5 h, based on conservative estimates of soil water content). Ks_{min} was used as the stabilised infiltration rate in the Philip formula. Soil texture was used in the pedotransfer function to assess soil porosity and bulk density (Saxton *et al*., 1986). Soil transmissivity T_{min} and T_{max} were

Table 1. Distribution of soil and land use areas by slope angle class expressed as km² and percentage.

		Slope angle class							
		0°-10°		10°-20°		20°-30°		>30°	
		%	km²	%	km²	%	km²	%	km²
Soil texture	Clay loam	23.0	32.0	36.3	50.5	66.4	92.3	75.6	105.1
	Loam	73.3	101.9	59.4	82.6	32.3	44.9	24.0	33.4
	Sand loam	3.7	5.1	4.3	6.0	1.3	1.8	0.4	0.6
Land use	Pasture	7.7	10.7	4.9	6.8	3.3	4.6	2.3	3.2
	Grain	67.2	93.5	61.5	85.5	40.7	56.5	23.4	32.5
	Mixed-forest	9.5	13.2	10.2	14.2	15.2	21.1	22.1	30.8
	Conifers	1.7	2.3	1.8	2.4	2.3	3.1	1.7	2.4
	Shrubs	13.9	19.3	21.6	30.0	38.5	53.5	50.4	70.1
	Hardwood-forest	0.0	0.0	0.1	0.1	0.1	0.1	0.1	0.1
Area	-	18.2	25.3	32.3	44.9	34.4	47.8	15.1	21.0

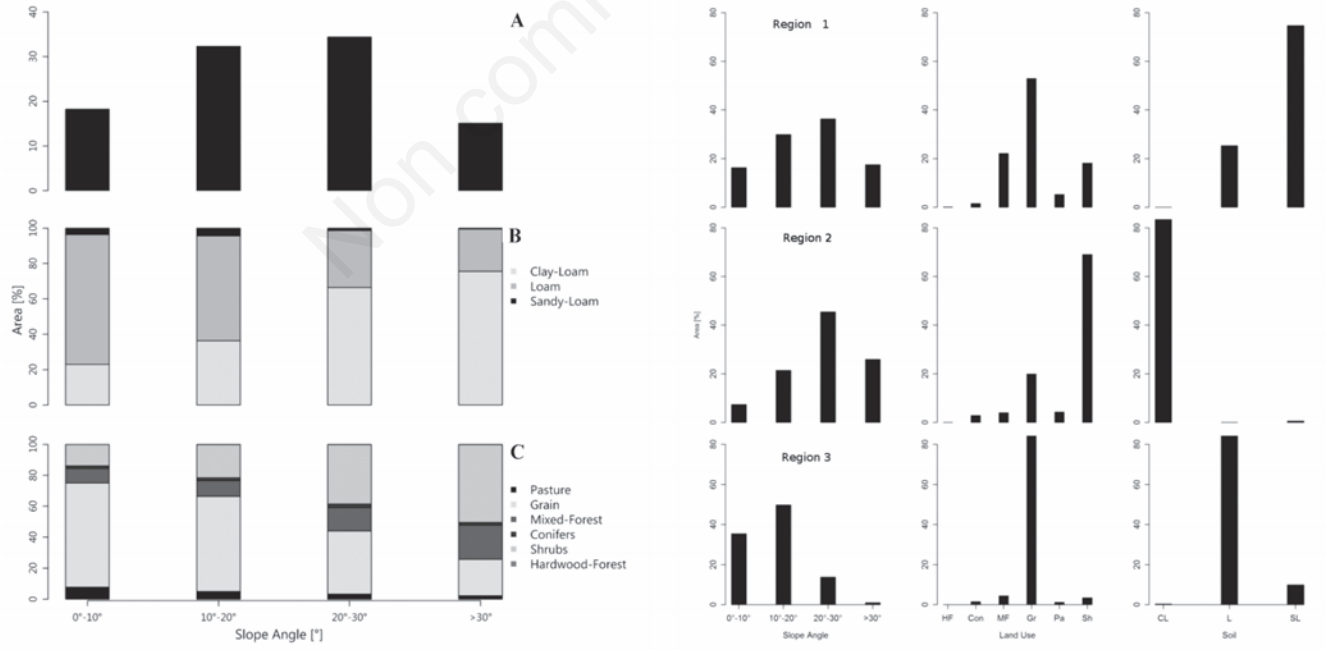

Figure 3. Left panel: Relative frequency distribution of slope angle classes in the study area (A) and bar-plots of soil classes and land use for each slope angle class (B and C). Right panel: Distribution of landslide-affecting factors for the three calibration regions expressed as a percentage. The x-axis shows slope angle classes, soil type (CL, clay loam; L, loam; SL, sand loam) and land use (Pa, pasture; Gr, grain; MF, mixed forest; Con, conifers; Sh, shrubs, HF, hardwood forest). The y-axis plots the area occupied expressed as percentage of the whole area of the calibration region.

calculated from the dataset provided by the soil depth map and the calculated values of Ks_{min} and Ks_{max}. Soil depth values derived from the soil map were used in Eq. 1 as the soil thickness parameter. These were consistent with landslide failure depths measured by the survey.

Geotechnical parameters were assessed from soil characteristics. Soil cohesion values were estimated for each of the defined soil classes. Root cohesion was assessed according to methods described in Preti *et al*. (2010), Preti and Giadrossich (2009) and Schwarz *et al*. (2009) and took into account root reinforcement at a depth of one meter for each class of land use. Root density distribution and consequently soil root reinforcement is assumed to be a decreasing exponential function of root depth (Preti *et al*., 2010). The estimated values of soil and root cohesion are used in Eq. 1 to calculate the cohesion index for each CR (Table 3). Minimum values for soil and root cohesion are assumed to be 0, in order to provide a conservative assessment of the risk of landslide. Maximum values were calculated as the weighted arithmetic average for the area covered following the procedure illustrated in Figure 2.

Model performance in a data-poor region

The success rate (SR) (Montgomery and Dietrich, 1994; Duan and Grant, 2000; Borga *et al*., 2002) evaluates the performance of the stability model. It is the ratio of the number of landslides that actually occur in areas that are predicted to be unstable divided by the total number of observed landslides. The SR does not take into account stable areas where predictions may or may not be correct. However, the SR indicator tends to over-predict slope failure. Consequently, Huang and Kao (2006) examined the successful prediction of landslides in stable areas and developed the modified success rate (MSR), which is the average success rate in predicting landslides in both stable and unstable areas. The landslide susceptibility map was verified using the success rate curve and the location of landslides mapped by Chung and Fabbri (2003). The success rate curve was plotted based on susceptibility classes, starting from highest to lowest values on the x-axis, and the cumulative percentage of landslide occurrence on the y-axis.

Results and discussion

The geospatial analysis, using the nearest neighbour method, showed a moderate landslide cluster distribution (P-value: 0.175), probably due to the small sample size (consistent with Yang and Lee, 2006).

The landslide inventory was evaluated by analysing the slope degree calculated from the DEM after digitalisation of the dataset. Figure 4 shows the slope angle (derived from the DEM) for each mapped landslide and the relative distribution frequency, for each slope class. Landslide frequency in areas with a slope angle of 0°-10°, 10°-20°, 20°-30° and >30° is 25%, 41.7%, 20.8% and 12.5%, respectively. This frequency distribution can be compared with landslide-triggering causes found in the landslide inventory, which suggests that localised processes could be the cause of some mapped landslides.

The graph shown in Figure 5 highlights the weak negative correlation between altitude and slope angle for mapped landslides. Although altitude does not directly affect the probability of a landslide, it can control several other factors, notably vegetation (Lan *et al*., 2004; Preti *et al*., 2010). The lack of vegetation at high altitude means that there is little or no root reinforcement causing a possible increasing slope exposure to extreme rainfall. This result could also be related to the practical difficulty of surveying high, steep zones. It should also be noted that the landslide inventory was focused on the socio-economic impacts of landslides. The SINMAP model was applied to the Comitancillo municipality in order to carry out an assessment of landslide hazard. We created a map of landslide hazard based on the input parameters shown in Table 3 and compared the results to the landslide inventory (Table 4). The results of the simulation indicated that 5.7% of the municipality was classified as *defended* (DEF), while 34.5% and 38.9% of the area were classified respectively as *upper threshold of instability* (UTS) and *lower threshold of instability* (LTS). The rest of the area (20.9%) was classified *quasi-stable, moderately stable* or *stable* (QS, MS and ST). The zones classified as DEF, UTS and LTS cover areas of 49.2 km^2, 43.6 km^2 and 7.2 km^2, respectively (Table 4). *Defended* areas lack stabilising factors.

Table 2. Distribution of factors affecting landslides for the three calibration regions.

		Region (km^2) 1	2	3
Land use	Hardwood forest	0.1	-	-
	Conifers	1.5	2.8	1.6
	Mixed forest	22.1	4.0	4.4
	Grain	53.0	19.9	89.3
	Pasture	5.2	4.2	1.2
	Shrubs	18.1	69.1	3.5
Soil type				
	Clay loam	-	99.5	0.3
	Loam	25.3	-	89.8
	Sand loam	74.7	0.5	9.9
Slope angle				
	0°-10°	16.3	7.3	35.4
	10°-20°	29.9	21.4	49.8
	20°-30°	36.3	45.4	13.8
	30°-40°	17.5	25.9	1.0

Table 3. Model input parameters for each calibration region.

			Region 1	Region 2	Region 3
Bulk density	kg/m^3		1520	1320	1430
Soil depth	cm		79	150	95
Hydraulic conductivity	cm/s	Ks min	6.01E-03	4.43E-03	5.26E-03
		Ks max	5.20	3.83	4.55
Root cohesion	N/m^2	Cr min	0	0	0
		Cr max	1601	1763	381
Soil cohesion	N/m^2	Cs min	0	0	0
		Cs max	3812	9566	6805
Wetness index	-	R/T min	2.8	1.9	1.8
		R/T max	28.4	40.0	29.9
Cohesion index	-	C min	0	0	0
		C max	0.37	0.43	0.42
Internal friction angle	°	ϕ min	27	23	27
		ϕ max	30	25	30

Figure 4 shows the relative frequency distribution of stability classes and mapped landslides. The area classified as DEF has relatively few mapped landslide events; this is probably due to the problem of localising landslides on steep slopes. Most mapped landslides (66.7%) are found in a zone where the SI is 1-0.5. Finally, 20.83% of all landslide events occurred in the area classified as ST (Table 4).

Figure 3B shows the distribution of soil classes for each slope angle. The percentage of clay loam increases as the slope angle increases (Figure 3B). On the other hand, the opposite trend is observed for loam, while there is no clear trend for sand loam. The positive correlation between clay loam and slope angle could be due to the cohesion effect of clay components. Figure 3C shows that the areas covered by hardwood forest, mixed forest and conifers do not show any clear trend in terms of slope angle, while areas covered by grains (*e.g.*, maize and beans) and shrubs reveal a clear correlation with slope angle. This correlation is negative for grain areas and positive for shrubs.

The survey data reports small-scale landslides in areas predicted by the model to be stable. Factors that trigger land movements could be linked to local situations (*e.g.*, slope toe erosion due to stream action). However, it has already been established that large-scale land movements caused by local characteristics cannot be evaluated with the infinite slope stability model based on a 20-metre DEM. In fact, a model's ability to assess the likelihood of shallow landslides is closely associated with the DEM resolution used for the simulation. Several authors have investigated the effects of DEM resolution on the topography index (Beven and Kirkby, 1979; Moore *et al*., 1991; Quinn *et al*., 1991; Band *et al*., 1993; Chairat and Delleur, 1993; Zhang and Montgomery, 1994; Saulnier *et al*., 1997) and landslide modelling (Ward, 1981; Borga *et al*., 1998, 2002; Claessens *et al*., 2005). The Claessens study concludes that low DEM resolution affects the quality of a model's results because features are *filtered out*. In our study, the effects of DEM resolution on landslide modelling were taken into account when results were compared with the landslide inventory.

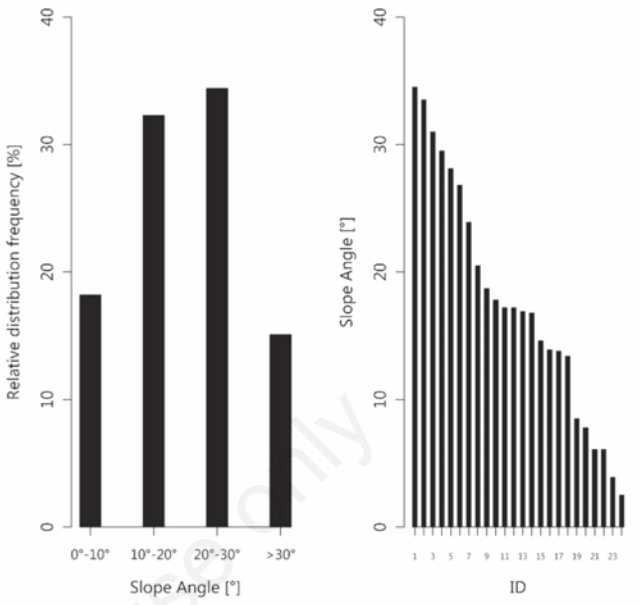

Figure 4. Relative distribution frequency for each slope class (left-hand side plot) and histogram of slope degree from the digital elevation model for mapped landslides.

Table 4. Study area classified according to stability hazard based on model simulation and distribution of mapped landslides in stability areas.

		Stable	Moderately stable	Quasi-stable	Lower threshold	Upper threshold	Defended	Total
Region 1	Area (km^2)	9.35	1.38	4.07	27.95	21.94	4.16	68.8
	% of region	13.58	2.01	5.91	40.6	31.87	6.04	100
	Landslides	1	0	2	4	2	0	9
	% of slides	11.11	0	22.22	44.44	22.22	0	100
Region 2	Area (km^2)	1.55	0.25	1.09	13.02	20.69	3.01	39.6
	% of region	3.92	0.63	2.75	32.88	52.23	7.6	100
	Landslides	1	0	1	3	3	0	8
	% of slides	12.5	0	12.5	37.5	37.5	0	100
Region 3	Area (km^2)	4.74	1.72	2.26	8.21	0.97	0.01	17.9
	% of region	26.49	9.58	12.63	45.86	5.41	0.03	100
	Landslides	3	0	0	3	1	0	7
	% of slides	42.86	0	0	42.86	14.29	0	100
Total	Area (km^2)	15.64	3.35	7.42	49.18	43.59	7.17	126.3
	% of area	12.38	2.65	5.87	38.92	34.5	5.67	100
	No. cells	39,100	8375	18,550	122,950	108,975	17,925	315,750
	Landslide	5	0	3	10	6	0	24
	% of slides	20.83	0	12.5	41.67	25	0	100
Total*	Area (km^2)	2.3	1.34	5.51	48.1	41.27	0.93	99.5
	% of area	2.31	1.35	5.54	48.36	41.5	0.94	100
	No. cells	5750	3350	13,775	120,250	103,175	2325	248,750
Total°	Area (km^2)			6.00	48.00	41.00		94.9
	% of area			5.81	50.69	43.5		100
	No. cells			15,000	120,000	102,500		237,250
Landslide#	Landslide			2	10	6		18
	% of slides			11.11	55.56	33.33		100

*Total=excluding areas with 10°>slope angle >35°; ° Total=excluding areas with 10°> slope angle >35°, in areas classified as quasi-stable slope, lower threshold slope and upper threshold slope; #Landslide=LS18.

Figure 6 highlights the relative frequency of mapped landslides (LS24), while LS18 is a sample of mapped landslides. Small-scale landslides were excluded, as the 20-metre DEM resolution used in the model was not able to identify landslide-triggering processes (see above). This reduction in the number of samples produced a 27% increase in the number of landslides mapped with an SI of 1-0.5. The distribution predicted by the model was compared to the landslide inventory (Table 5). In simulation of model results (MR) 2, areas with a slope angle less than 10° or greater than 35° were excluded as the survey focused on areas closest to the village and therefore most dangerous for populations, and did not include inaccessible areas.

The Chi-square test for the comparison of two samples with homogenous variance and unknown population variance was applied (Table 5). The same table also shows that calculated P-values for the Chi-square test increase from 0.977 to 0.993 for samples LS24-MR1 and LS18-MR2 respectively. In these two cases the average of the sample pairs are similar, in particular for LS18-MR2. These results show that, when compared with the survey inventory, the SINMAP model provides reliable results from the statistical estimate of input parameters.

The SR indices for LS24-MR1 and LS18-MR2 are respectively 67% and 89%. Figure 6 plots the success rate curve, which shows the percentage distribution of mapped landslides in areas of different susceptibility classes.

Figure 6 shows a clear correlation between the distribution of mapped landslides and areas with highest SI, as calculated by the model. The presence of mapped landslides in areas with an SI less than 1.5 is probably due to local characteristics.

The MSR index was not used for two reasons: i) the landslide inventory only provided a sample of mapped landslides in the study area; and

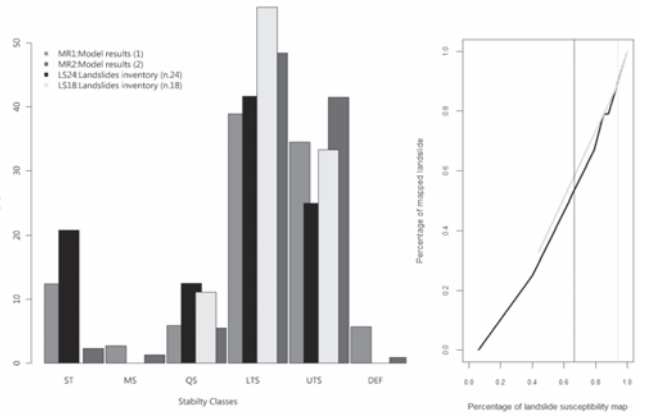

Figure 6. Left panel: Relative distribution frequency for the model output compared to the landslide inventory. The relative frequency distribution of areas classified according to the stability classes defined by the model (M1) and the relative frequency distribution of the 24 mapped landslides for each stability class were plotted. M2 shows the distribution of areas classified according to the stability classes defined by the model excluding areas with slope angle less than 10° or greater than 35°. LS18 shows a sample of mapped landslides excluding small-scale landslides. Right panel: Success rate curve plotted for the two samples (LS18, grey curve; LS24, black curve) of selected landslides. Vertical lines show the zone of the plot (on the left) of susceptible areas. ST, stable slope; MS, moderately stable slope; QS, quasi-stable slope; LTS, lower threshold slope; UTS, upper threshold slope; DEF, defended slope.

Table 5. Chi-square test results and success rate index of model output and landslide inventory.

Case	x-square	df	P-value	SR
LS24-MR1	0.204	3	0.977	67%
LS18-MR2	0.0821	3	0.993	89%

df, degree of freedom; SR, success rate.

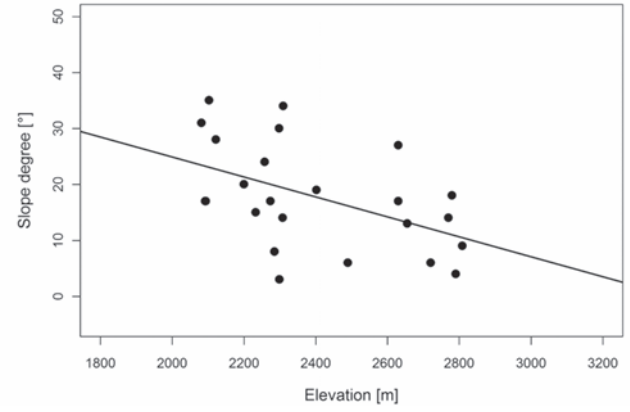

Figure 5. Slope angle (calculated from the digital elevation model) and altitude of mapped landslides.

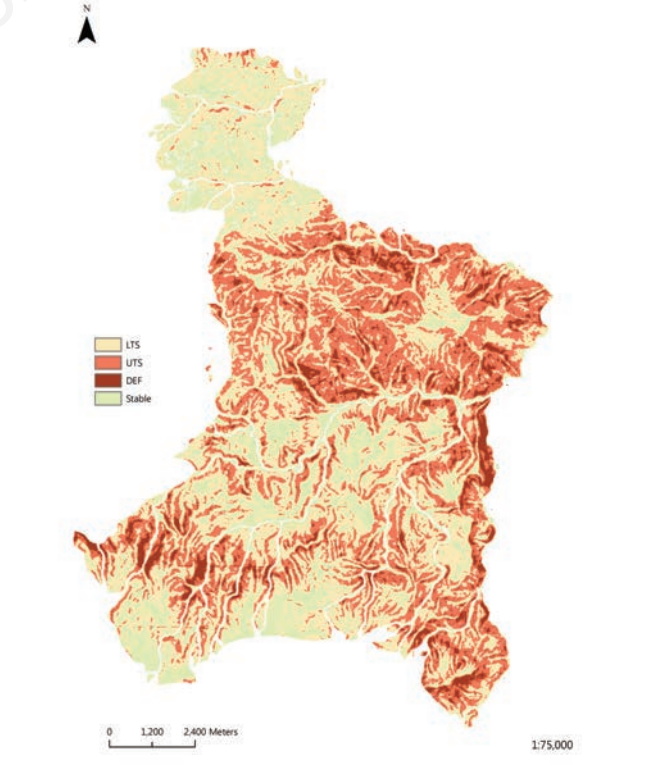

Figure 7. Stability index map calculated by the stability index mapping with a reclassification of stability classes as follows: DEF, defendable; UTS, upper threshold slope zone; LTS, lower threshold slope zone; Stable, quasi-stable slope zone + moderately stable zone + stable slope zone.

ii) it is not possible to assume that each landslide only occupies one cell in a grid of 20-metres or more.

The first type of error in modelling slope stability occurs when the model identifies a site as unstable, but no evidence of instability can be observed or mapped. The second type of error occurs when a site is predicted to be stable but instability is observed (Borga *et al*., 2002). The first type of error tends to over-predict areas that may be subject to shallow landslides, but could also be an indication that the zone is prone to instability. The second type of error suggests that the model does not accurately describe instabilities, which are minimised (as was the case in this study).

The implementation described here offers a reliable method for the mapping of shallow landslide susceptibility in data-poor regions (Figure 7).

Conclusions

A deterministic model (SINMAP) was applied to the Comitancillo municipality in Guatemala to assess landslide hazard. The study area (139 km^2) was divided into three calibration regions according to their geotechnical characteristics. The aim was to evaluate the usefulness of the simulations provided by the SINMAP model in data-poor regions, through a comparison of the model's results with an inventory of observed landslides. The model's input parameters were derived from a statistical analysis of landslide-affecting factors. Geotechnical data for the model's calibration regions were estimated from a soil map. Root reinforcement was assessed from a vegetation cover map of the area. The model was validated using a sample of 24 observed landslides.

The results of the simulation showed that around 79% of the municipality could be classified as between the *lower threshold of* instability and *defended*.

The landslide inventory is a partial sample of shallow landslides in Comitancillo municipality and includes small land movements. However, the 20-metre DEM used in our simulation is not able to identify these small-scale movements, especially when they are triggered by local characteristics.

The validation of the model shows that the data input procedure makes it possible to carry out a reliable simulation of scenarios to assess the likelihood of shallow landslides. In particular, the SINMAP model can be applied in data-poor regions where landslides are not caused or triggered by local characteristics.

The susceptibility map is a tool that planners can use to ensure that areas prone to landslide are used in ways that reduce the probability of a harmful event or to mitigate its effects. Finally, it can also be used to identify existing infrastructure (terracements, roads, *etc*.) subject to landslide hazard (Tarolli *et al*., 2013).

References

Andriola P., Chirico G.B., De Falco M., Di Crescenzo G., Santo A. 2009. Comparison between physically-based models and a semiquantitative methodology for assessing susceptibility to flowslides triggering in the pyroclastic deposits oh southern Italy. Geogr. Fisica Dinam. Quat. 32:213-26.

Band L.E., Patterson P., Nemani R., Running S.W. 1993. Forest ecosystem processes at the watershed scale: incorporating hillslope hydrology. Agric. Forest Meteorol. 63:93-126.

Barling R.D., Moore I.D., Grayson R.B. 1994. A quasi-dynamic wetness index for characterizing the spatial distribution of zones of surface saturation and soil water content. Water Resour. Res. 30:1029-44.Bathurst J.C., Moretti G., El-Hames A., Begueria S., Garcia-Ruiz J.M. 2007. Modelling the impact of forest loss on shallow landslide sediment yield, Ijuez river catchment, Spanish Pyrenees. Hydrol. Earth Syst. Sci. 11:569.

Baum R.L., Godt J.W., Savage W.Z. 2010. Estimating the timing and location of shallow rainfall-induced landslides using a model for transient, unsaturated infiltration. J. Geophys. Res. Earth Surf. 115:F03013.

Baum R.L., Savage W.Z., Godt J.W. 2002. TRIGRS - A FORTRAN program for transient rainfall infiltration and grid-based regional slope-stability analysis. U.S. Geological Survey Open-File Report 02-0424, 35 pp. Available from: http://pubs.usgs.gov/of/2002/ofr-02-424/

Baum R.L., Savage W.Z., Godt J.W. 2008. TRIGRS: a Fortran program for transient rainfall infiltration and grid-based regional slope-stability analysis, version 2.0. U.S. Geological Survey Open-File Report, 2008-1159, 75 pp. Available from: http://pubs.usgs.gov/of/2008/1159/

Beven K.J., Kirkby M.J. 1979. A physically based, variable contributing area model of basin hydrology. Hydrol. Sci. Bull. 24:43-69.

Borga M., Dalla Fontana G., Da Ros D., Marchi L. 1998. Shallow landslide hazard assessment using a physically based model and digital elevation data. J. Environ. Geol. 35:81-8.

Borga M., Dalla Fontana G., Gregoretti C., Marchi L. 2002. Assessment of shallow landsliding by using a physically based model of hillslope stability. Hydrol. Process. 16: 2833-51.

Bresci E, Giacomin A, Preti F. 2013. Experiences of improving water access in rural areas in Guatemala. J. Agric. Engine. 2013; 44(s2):e171.

Calcaterra D., de Riso R., Di Martire D. 2004. Assessing shallow debris slide hazard in the Agnano Plain (Naples, Italy) using SINMAP, a physically based slope-stability model. In: W.A. Lacerda, M.E. Ehrlich, S.A.B. Fontoura, A.S.F. Sayao (Eds.), Landslides: evaluation and stabilization. Taylor and Francis Group, London, UK, 1:177-183.

Cepeda J., Höeg K., Nadim F. 2010, Landslide-triggering rainfall thresholds: a conceptual framework. Q. J. Engine. Geol. Hydrogeol. 43:69–84.

Chairat S., Delleur J.W. 1993. Effects of topographic index distribution on predicted runoff using GRASS. Water Resour. Bull. 29:1029-34.

Chirico G.B., Grayson R.B., Western A.W. 2003. On the computation of the quasi-dynamic wetness index with multiple-flow-direction algorithms. Water Resour. Res. 39:1115.

Chirico G.B., Medina H., Romano N. 2010. Functional evaluation of PTF prediction uncertainty: An application at hillslope scale. Geoderma 155:193-202.

Chung C.F., Fabbri A.G. 2003. Validation of spatial prediction models for landslide hazard mapping. Nat. Hazard 30:451-72.

Claessens L., Heuvelink G.M.B, Schoorl J.M., Veldkamp A. 2005. DEM resolution effects on shallow landslide hazard and soil redistribution modeling. Earth Surf. Process. Landforms 30:461-47.

Coe J.A., Godt J.W., Baum R.L., Bucknam R.C., Michael J.A. 2004. Landslide susceptibility from topography in Guatemala. In: W.A. Lacerda, M.E. Ehrlich, S.A.B. Fontoura, A.S.F. Sayao (Eds.), Landslides-evaluation and stabilization, Proc. 9th Int. Symp. Landslides. A.A. Balkema Publishers, London, UK, 1:69-78.

Connell L.D., Jayatilaka C.J., Nathan R. 2001. Modelling flow and transport in irrigation catchments, spatial application of subcatchment model. Water Resour. Res. 37:965-77.

Cosby B.J., Hornberger G.M., Clapp R.B., Ginn T.R. 1984. A statistical exploration of the relationship of soil moisture characteristics to the physical properties of soils. Water Resour. Res. 20:682-90.

Deb S.K., El-Kadi A.I. 2009. Susceptibility assessment of shallow landslides on Oahu, Hawaii, under extreme-rainfall events. Geomorphology 108:219-33.

Devoli G., Cepeda J., Kerle N. 2009. The 1998 Casita volcano flank fail-

ure revisited: new insights into geological setting and failure mechanisms. Engine. Geol. 105:65-83.
Devoli G., Morales A., Høeg K. 2007a. Historical landslides in Nicaragua-collection and analysis of data. Landslides. 4:5-18.
Devoli G., Strauch W., Chávez G., Høeg K. 2007b. A landslide database for Nicaragua: a tool for landslide hazard management. Landslides. 4:163-76.
Dietrich E.W., Bellugi D., Real De Asua R. 2001. Validation of shallow landslide model, SHALTAB, for forest management. In: M.S. Wigmosta and S.J. Burges (Eds.), Land use and watersheds: human influence on hydrology and geomorphology in urban and forest areas - Water Science and Application Series. American Geophysical Union, Washington, DC, USA, 2:195-227.
Dietrich W.E., Montgomery D.R. 1998. SHALSTAB: a digital terrain model for mapping shallow landslide potential. University of California and University of Washington, Berkeley, CA, USA.
Dietrich E.W., Reisss R., Hsu M.L., Montgomery D.R. 1995. A process-based model for colluvial soil depth and shallow landsliding using digital elevation data. Hydrol. Process. 9:383-400.
Dietrich W.E., Wilson C.J., Montgomery D.R., McKean J., Bauer R. 1992. Erosion thresholds and land surface morphology. Geology 20:675-9.
Dietrich W.E., Wilson C.J., Montgomery D.R., McKean J. 1993. Analysis of erosion thresholds, channel networks, and landscape morphology using a digital terrain model. J. Geol. 101:259-78.
Duan J., Grant G.E. 2000. Shallow landslide delineation for steep forest watershed based on topographic attributes and probability analysis. In: J.P. Wilson and J.C. Gallant (Eds.), Terrayn analysis: principles and applications. Wiley, New York, NY, USA, pp 311-329.
Ghosh S., van Westen C.J., Carranza E.J.M., Jetten V.G., Cardinali M., Rossi M., Guzzetti M. 2012. Generating event-based landslide maps in a data-scarce Himalayan environment for estimating temporal and magnitude probabilities. Engine. Geol. 128:49-62.
Glade T. 2003. Landslide occurrence as a response to land use change: a review of evidence from New Zealand. Catena. 51:297-314.
Greenway D.R. 1987. Vegetation and slope stability. In: M. Gerson and K.S. Richards (Eds.), Slope stability. John Wiley & Sons, Chichester, UK, pp 187-230.
Huang J.C., Kao S.J. 2006. Optimal estimator for assessing landslide model efficiency. Hydrol. Earth Syst. Sci. Discuss. 3:1125-44.
INSIVUMEH. 1991. Inventario de los principales deslizamientos ocurridos en la República de Guatemala. Instituto Nacional de Sismología, Vulcanología, Meteorología e Hidrología, Guatemala City, Guatemala.
Iverson R.M. 2003. How should mathematical models of geomorphic processes be judged? In: P.R. Wilcock and R.M. Iverson (Eds.), Prediction in geomorphology - geophysical monograph 135. American Geophysical Union, Washington, DC, USA, pp 83-94.
Jaiswal P., van Westen C.J. 2013. Use of quantitative landslide hazard and risk information for local disaster risk reduction along a transportation corridor: a case study from Nilgiri district, India. Nat. Hazards 65:887-913.
Kuriakose S.L., van Beek L.P.H., van Westen C.J. 2009. Parameterizing a physically based shallow landslide model in a data poor region. Earth Surf. Process. Landforms 34:867-81.
Lan H.X., Zhou C.H., Wang L.J., Zhang H.Y., Li R.H. 2004. Landslide hazard spatial analysis and prediction using GIS in the Xiaojiang watershed, Yunnan, China. Eng. Geol. 76:109-28.
Li Y.H. 1988. Denudation rates of the Hawaiian Islands by rivers and groundwaters. Pac. Sci. 42:253-66.
MAGA (Ministerio de Agricultura, Ganaderia y Alimentacion). 2001. Base de datos digital de la Republica de Guatemala a escala 1:250,00; Junio, 2001. Guatemala City, Guatemala.
Medina B.Y. 2007. Deslizamiento y impactos ambientales de los huracanes Mitch y Stan, en Guatemala. Jornadas Internacionales sobre Gestión del Riesgo de Inundaciones y Deslizamientos de Laderas, Mayo 2007, Brasil.
Meisina C., Scarabelli S. 2007. A comparative analysis of terrain stability models for predicting shallow landslides in colluvial soils. Geomorphology 87:207-23.
Miner Y.F., Villagran de Leon J.C. 2008. Managing landslides in Guatemala, critical issues. pp 45-48 1st World Landslide Forum, Session 03, 18-21 November 2008, United Nations University, Tokyo, Japan.
Montgomery D.R., Dietrich W.E. 1994. A physically based model for the topographic control on shallow landsliding. Water Resour. Res. 30:1153-71.
Montgomery D.R., Schmidt K.M., Green Berg H.M., Dietrich W.E. 2000. Forest clearing and regional landsliding. Geology 28:311-4.
Moore I.D., Grayson R.B., Ladson A.R. 1991. Digital terrain modeling: a review of hydrological, geomorphological and biological applications. Hydrol. Process. 5:3-30.
Morrissey M.M., Wieczorek G.F., Morgan B.A. 2001. A comparative analysis of hazard models for predicting debris flows in Madison County, Virginia. Open File Report 01-0067. U.S. Geological Survey. Available from: http://pubs.usgs.gov/of/2001/ofr-01-0067/ofr-01-0067.html
Pack R.T., Tarboton D.G., Goodwin C.N. 1998. In: D.P. Moore and O. Hungr (Eds.), The SINMAP approach to terrain stability mapping. Proc. 8th Congr. International Association of Engineering Geology and the Environment, A. A. Balkema, Rotterdam, the Netherlands, 2:1157-1165.
Pellicani R., van Westen C.J., Spilotro G. 2013. Assessing landslide exposure in areas with limited landslide information. Landslides 11:463-80.
Petley D.N., Dunning S.A., Rosser N.J. 2005. The analysis of global landslide risk through the creation of a database of worldwide landslide fatalities. In: O. Hungr, R. Fell, R. Couture, E. Eberhardt (Eds.), Landslide risk management. Balkema, Rotterdam, the Netherlands, pp 367-374.
Philip J.R. 1957. The theory of infiltration: 1. The infiltration equation and its solution. Soil Sci. 83:34-57.
Preti F. 2013. Forest protection and protection forest: tree root degradation over hydrological shallow landslides triggering. Ecol. Engine. 61P:633-45.
Preti F., Dani A., Laio F. 2010. Root profile assessment by means of hydrological, pedological and above-ground vegetation information for bio-engineering purposes. Ecol. Eng. 36:305-16.
Preti F., Giadrossich F. 2009. Root reinforcement and slope bioengineering stabilization by Spanish Broom (Spartium junceum L.). Hydrol. Earth Syst. Sci. 13:1713-26.
Preti F., Tarolli P., Dani A., Calligaro S., Prosdocimi M. 2013. LiDAR derived high resolution topography: the next challenge for the analysis of terraces stability and vineyard soil erosion. J. Agric. Engine. 44:(s2):85-9.
Quinn P., Beven K., Chevallier P., Planchon O. 1991. The prediction of hillslope flow paths for distributed hydrological modelling using digital terrain models. Hydrol. Process. 5:59-79.
Santacana N., Baeza B., Corominas J., De Paz A., Marturia J. 2003. A GIS-based multivariate statistical analysis for shallow landslide susceptibility mapping in La Pobla de Lillet Area (Eastern Pyrenees, Spain). Nat. Hazards 30:281-95.
Saxton K.E., Rawls W.J., Romberger J.S., Papendick R.I. 1986. Estimating generalized soil-water characteristics from texture. Soil Sci. Soc. Am. J. 50:1031-6.
Saulnier G., Obled C., Beven K. 1997. Analytical compensation between DTM grid resolution and effective values of saturated hydraulic

conductivity within the TOPMODEL framework. Hydrol. Process. 11:1331-46.
Schwarz M., Preti F., Giadrossich F., Lehmann P., Or D. 2009. Quantifying the role of vegetation in slope stability: a case study in Tuscany (Italy). Ecol. Eng. 36:285-91.
Scott G.A.J, Street J.M. 1976. The role of chemical weathering in the formation of Hawaiian amphitheatre-headed valleys. Geomorphol. 20:171-89.
Simmons C.S., Tárano J.M., Pinto J.H. 1959. Clasificación de reconocimiento de los suelos de la república de Guatemala. Ed. José de Pineda Ibarra, Guatemala.
Tarolli P., Calligaro S., Cazorzi F., Dalla Fontana G. 2013. Recognition of surface flow processes influenced by roads and trails in mountain areas using high-resolution topography. Eur. J. Remote Sensing 46:176-97.
Terlien T.J. 1997. Hydrological landslide triggering in ash-covered slopes of Manizales (Colombia). Geomorphol. 20:165-75.
UNEP (United Nations Environment Programme). 2005. Hurricane Stan: environmental impacts from floods and mudslides in Guatemala results from a rapid environmental assessment in Guatemala joint. United Nations Office for the United Nations and Coordination of Humanitarian Affairs Environment Programme. Available from: https://docs.unocha.org/sites/dms/Documents/Guatemala_REA_261005_Final.pdf
van Beek L.P.H., van Asch T.W.J. 2004. Regional assessment of the effects of land-use change and landslide hazard by means of physically based modelling. Nat. Hazards 30:289-304.
Ward T.J. 1981. Use of a mathematical model for estimating potential landslide sites in steep forested drainage basins. pp 21-41 in Erosion and sediment transport in pacific rim steeplands. IAHS Publication 132. IAHS, Christchurch, UK.
Wentworth C.K. 1943. Soil avalanches on Oahu, Hawaii. Bull. Geol. Soc. Am. 54:53-64.
Wu W., Sidle R.C. 1995. A distributed slope stability model for steep forested watersheds. Water Resour. Res. 31:2097-211.
Yang Z.-Y., Lee Y.-H. 2006. The fractal characteristics of landslides induced by earthquakes and rainfall in central Taiwan. IAEG2006 Paper number 48. 10th IAEG International Congress, Nottingham, UK.
Zaitchik B.F., van Es H.M. 2003. Applying a GIS slope-stability model to site-specific landslide prevention in Honduras. J. Soil Water Conserv. 58:45-53.
Zhang W., Montgomery D.R. 1994. Digital elevation model grid size, landscape representation, and hydrologic simulations. Water Resour. Res. 30:1019-28.